Stopband-Extended and Size-Miniaturized Low-Pass Filter with Three Transmission Zeros

Lin Li, Jia Bao, Jing-jing Du, and Yaming Wang

This paper presents a compact structure composed of an upper high-impedance transmission line, a middle extended parallel coupled line, and a pair of inter-coupled symmetrical stepped impedance stubs. Detailed investigation into this structure based on an equivalent circuit analysis reveals that this proposed structure exhibits a quasi-elliptic low-pass filtering response with three transmission zeros. Moreover, the positions of the three transmission zeros can be tuned and reallocated flexibly by choosing the proper circuit parameters. Finally, the design concept is validated through the design, fabrication, and measurement of two exemplary low-pass filters (LPFs) with one single unit and two cascaded asymmetric units. The measured results agree well with the simulated results. In addition, in the range of 1.42 f_c to 7.03 f_c, the fabricated quasi-elliptic LPFs experimentally demonstrate a very wide upper-stopband of 20 dB using a compact size of only 0.0089λ_g^2, where λ_g is the guided wavelength of a 50 Ω transmission line at the central frequency.

Keywords: Low-pass filter (LPF), transmission zero, wide stopband, compact size

I. Introduction

Microwave low-pass filters (LPFs) are frequently required in many types of wireless communication systems to suppress unwanted harmonics and spurious signals. Conventional LPFs adopting a stepped-impedance configuration cannot meet the requirements of modern communication systems because of their large size and narrow stopband [1]. Therefore, new LPFs with a compact size, low insertion loss, and wide stopband are highly desirable today.

To address the above mentioned problems, many methods have been recently proposed. To obtain wide stopband low-pass filtering responses, different electromagnetic band-gap (EBG) structures are employed in [2]. However, it is well known that the periodic characteristic of an EBG causes a very large size. Defected ground structures (DGSs) have also been used in [3] and [4] to obtain a performance-improved LPF. However, a minimum air-space volume beneath the ground plane is required for the structure to function effectively. Additionally, these DGS structures with an aperture etched on the ground plane bring about many other disadvantages such as complex configuration and fabrication difficulties. Different structures with multiple transmission zeros are also employed to create an elliptic-function low-pass response with a wider stopband. In [5], elliptic-function LPFs based on microstrip stepped-impedance hairpin resonators have been presented by creating two coupling routes between non-adjacent sections. However, the filter transition in [5] is still gradual since the only transmission zero is far from the cutoff frequency. Different LPF topologies with two transmission zeros have also been investigated in [6]-[8]. However, since only two transmission zeros are provided, these filters are unavailable for the application when a wide and high-rejected stopband are

Manuscript received Apr. 30, 2013; revised Aug. 15, 2013; accepted Aug. 21, 2013.

This work was supported by the National Natural Science Foundation of China under grants (61101052, 61070063), Zhejiang Provincial Natural Science Foundation under grants (Y1110297).

Lin Li (phone: +86 571 86843325, lilin_door@hotmail.com), Jia Bao (baojia@zstu.edu.cn), Jing-jing Du (Jingjdu@163.com), and Yaming Wang (ywang@zist.edu.cn) are with the Department of Electronics, Zhejiang Sci-Tech University, Hangzhou, China.

required. Though multi-section structures composed of two asymmetrical cascaded units are employed in [7] and [8] to expand the stopband, this will greatly increase the filter size and design complexity. To generate more transmission zeros, a tightly coupled hairpin unit [9] and a capacitive loaded anti-coupled line [10] are presented to realize an LPF with three transmission zeros. However, the narrow zero-separation of the LPF in [9] and the larger size in [10] seriously limit their application. More than three transmission zeros using a stub-loaded coupled-line hairpin resonator are generated in [11]. However, several fluctuations in the stopband result in a significant deterioration of the stopband-rejection performance of an LPF.

In this paper, a compact structure is proposed to construct LPFs with an improved stopband performance. The investigation of this structure based on an equivalent circuit analysis reveals that this proposed structure exhibits a quasi-elliptic low-pass filtering response with three transmission zeros. Moreover, the mechanism for reallocating and adjusting the transmission zeros is also explained in detail. It was found that a larger zero separation can be easily achieved by choosing the proper circuit parameters. A simultaneously sharpened, high-rejected, and expanded stopband can thus be obtained. Finally, two LPFs using a single unit and two asymmetrical units, respectively, were optimally designed. The measured results agree well with the simulation results. Both the simulations and measurements of the two fabricated filters exhibit a good quasi-elliptic low-pass response including a sharp skirt, a lower passband insertion loss, an expanded stopband, and a compact size.

II. Filter Theory

Figure 1 shows a schematic of the proposed LPF. Assuming the structure is lossless that and all discontinuity effects can be neglected, the proposed structure can be divided into three shunt networks: one is the upper high-impedance transmission line, shown in Fig. 2; another is a mid-extended parallel coupled line, shown in Fig. 3; and the lower one is a pair of inter-coupled symmetrical stepped-impedance stubs, shown in Fig. 4.

As shown in Fig. 2, the upper single transmission line with a characteristic impedance of Z_{0u} and a length of l_u can be modeled as an equivalent L-C π-network. For this upper lossless transmission line, the ABCD matrix is given by

$$\begin{cases} A_u = \cos(\beta_u l_u), \\ B_u = jZ_{0u}\sin(\beta_u l_u), \\ C_u = jY_{0u}\sin(\beta_u l_u), \\ D_u = \cos(\beta_u l_u), \end{cases} \quad (1)$$

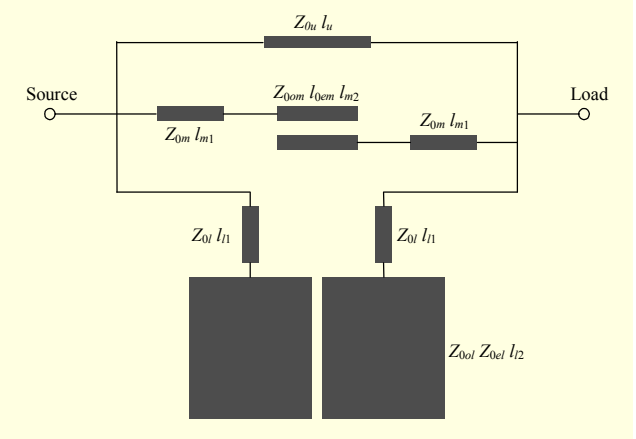

Fig. 1. Schematic of proposed LPF.

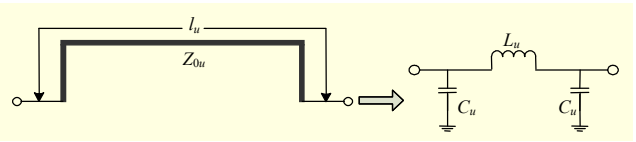

Fig. 2. Equivalent circuit of upper single transmission line.

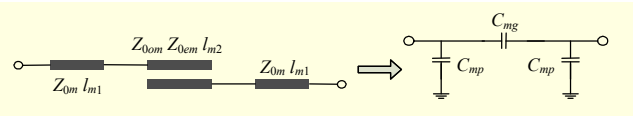

Fig. 3. Equivalent circuit of midsection.

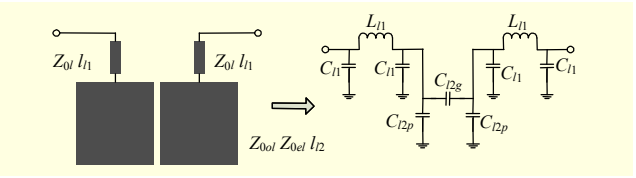

Fig. 4. Equivalent circuit of lower section.

where β_u and $Y_{0u} = 1/Z_{0u}$ are the phase constant and characteristic admittance of the single transmission line, respectively. In addition, the equivalent inductance and capacitance of the lumped π-network circuit are given by [5]

$$L_u = \frac{Z_{0u}\sin(\beta_u l_u)}{\omega}, \quad (2)$$

$$C_u = \frac{1-\cos(\beta_u l_u)}{\omega Z_{0u}\sin(\beta_u l_u)}. \quad (3)$$

For the mid-extended parallel coupled line, the total ABCD matrix is obtained as [1]

$$\begin{cases} A_m = A_1^2 A_2 + A_1 B_1 C_2 + A_1 C_1 B_2 + B_1 C_1 A_2, \\ B_m = 2A_1 B_1 A_2 + B_1^2 C_2 + A_1^2 B_2, \\ C_m = 2A_1 C_1 A_2 + A_1^2 C_2 + C_1^2 B_2, \\ D_m = A_1^2 A_2 + A_1 B_1 C_2 + A_1 C_1 B_2 + B_1 C_1 A_2, \end{cases} \quad (4)$$

where

$$\begin{cases} A_1 = \cos(\beta_m l_{m1}),\ B_1 = jZ_{0m}\sin(\beta_m l_{m1}), \\ C_1 = j\sin(\beta_m l_{m1})/Z_{0m},\ A_2 = \dfrac{Z_{0em}+Z_{0om}}{Z_{0em}-Z_{0om}}, \\ B_2 = -j\dfrac{2Z_{0em}Z_{0om}\cot(\beta_m l_{m2})}{(Z_{0em}-Z_{0om})},\ C_1 = j\dfrac{2\tan(\beta_m l_{m2})}{Z_{0em}-Z_{0om}}. \end{cases}$$

The mid-section can also be represented by the lumped π-network circuit in Fig. 3, and the equivalent capacitance of C_{mg} and C_{mp} can be given by

$$C_{mg} = 1/(j\omega B_m), \tag{5}$$

$$C_{mp} = (A_m - 1)/(j\omega B_m). \tag{6}$$

The lower section in Fig. 4 consists of one cascaded structure composed of two bilateral high-impedance transmission lines and one symmetric parallel coupled-line. For the bilateral transmission line with a characteristic impedance of Z_{0l} and a length of l_{l1}, the ABCD matrix is given by

$$\begin{cases} A_{l1} = \cos(\beta_{l1} l_{l1}), \\ B_{l1} = jZ_{0l}\sin(\beta_{l1} l_{l1}), \\ C_{l1} = j\sin(\beta_{l1} l_{l1})/Z_{0l}, \\ D_{l1} = \cos(\beta_{l1} l_{l1}), \end{cases} \tag{7}$$

where β_{l1} is the phase constant of the bilateral transmission line. This transmission line can be represented by the lumped π-network circuit in Fig. 4. In addition, the equivalent inductance and capacitance [5] are given by

$$L_{l1} = \frac{Z_{0l}\sin(\beta_{l1} l_{l1})}{\omega}, \tag{8}$$

$$C_{l1} = \frac{1-\cos(\beta_{l1} l_{l1})}{\omega Z_{0l}\sin(\beta_{l1} l_{l1})}. \tag{9}$$

For the symmetric parallel low-impedance coupled-line with odd- and even-mode characteristic impedances of Z_{0ol} and Z_{0el}, and a length of l_{l2}, the ABCD matrix of the lossless parallel coupled-line [1], [5] can be expressed as

$$\begin{cases} A_{l2} = \dfrac{Z_{0el}+Z_{0ol}}{Z_{0el}-Z_{0ol}}, \\ B_{l2} = -j\dfrac{2Z_{0el}Z_{0ol}\cot(\beta_{l2} l_{l2})}{Z_{0el}-Z_{0ol}}, \\ C_{l2} = j\dfrac{2\tan(\beta_{l2} l_{l2})}{Z_{0el}-Z_{0ol}}, \\ D_{l2} = \dfrac{Z_{0el}+Z_{0ol}}{Z_{0el}-Z_{0ol}}, \end{cases} \tag{10}$$

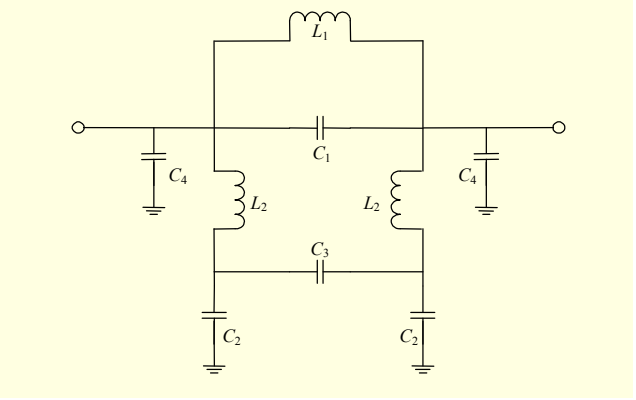

Fig. 5. Equivalent lumped model of the proposed structure.

where β_{l2} is the phase constant of the lower coupled lines. The equivalent π-network lumped model can be obtained as shown in Fig. 4, and the capacitances of the π-network are found [5] as

$$C_{l2g} = \frac{Z_{0el}-Z_{0ol}}{2\omega_0 Z_{0el}Z_{0ol}\cot(\beta_{l2} l_{l2})}, \tag{11}$$

$$C_{l2p} = \frac{1}{\omega_0 Z_{0el}\cot(\beta_{l2} l_{l2})}. \tag{12}$$

Furthermore, if the discontinuity effects are ignored, the lumped equivalent circuit of the proposed structure is shown in Fig. 5 by combining the above derived equivalent circuits of the three single sections, where $L_1 = L_u$, $C_1 = C_{mg}$, $L_2 = L_{l1}$, $C_2 = C_{l1} + C_{l2p}$, $C_3 = C_{l2g}$, and $C_4 = C_u + C_{mp} + C_{l1}$. To gain insight into this structure, we first assume $C_3 = 0$, which is a reasonable approximation since $C_3 << C_2$ for a loose coupled-line. When C_3 is removed, the model in Fig. 5 can be considered as a three-pole LC LPF.

In addition, as observed from the simplified model, two transmission zeros positioned at f_{z1} and f_{z2} are generated as the result of the parallel resonance between L_1 and C_1 and serial resonance between L_2 and C_2. Clearly, f_{z1} and f_{z2} can be derived as

$$f_{z1} = 1/(2\pi\sqrt{L_1 C_1}), \tag{13}$$

$$f_{z2} = 1/(2\pi\sqrt{L_2 C_2}). \tag{14}$$

Let $f_{z1} > f_{z2}$ by choosing the appropriate L_1, C_1, L_2, and C_2, and the transmission zero at f_{z2} then creates a sharpened transition, and the transmission zero at f_{z1} contributes to the stopband expansion. Clearly, a larger transmission zero separation will help to sharpen and extend the stopband. However, the stopband rejection between two transmission zeros is also deteriorated with an increase in the zero separation since only two transmission zeros exist. To obtain a sharpened, extended, and high-rejected stopband, C_3 is introduced to

ETRI Journal, Volume 36, Number 2, April 2014
http://dx.doi.org/10.4218/etrij.14.0113.0430

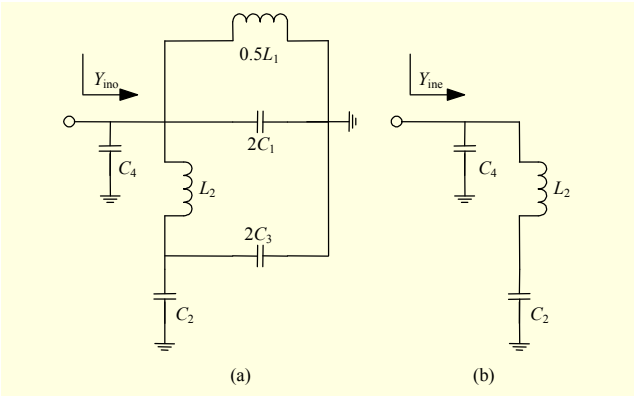

Fig. 6. Equivalent circuit of proposed filter: (a) odd-mode and (b) even-mode.

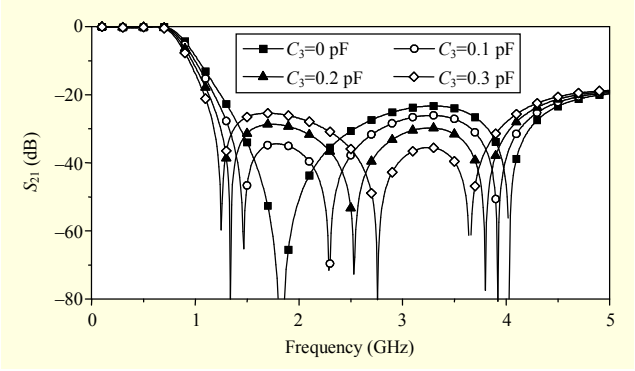

Fig. 7. Theoretical transmission responses of the LPF with different $C3$.

create an extra transmission zero between f_{z1} and f_{z2}. To gain insight into the effect of C_3 on the structure's response, the odd- and even-mode analysis method is employed to investigate this filter by utilizing the symmetry of the equivalent model. The equivalent odd- and even-mode circuits are given in Figs. 6(a) and 6(b), which were obtained from the replacement of the reference plane with magnetic and electric walls, respectively.

$$Y_{ino} = \frac{2}{j\omega L_1} + 2j\omega C_1 + j\omega C_4 + \frac{1}{j\omega L_2 + \frac{1}{j\omega C_2 + 2j\omega C_3}}, \quad (15)$$

$$Y_{ine} = j\omega C_4 + \frac{1}{j\omega L_2 + \frac{1}{j\omega C_2}}. \quad (16)$$

Clearly, C_3 exerts an effect on Y_{ino}, but has no effect on Y_{ine}. Network theory [1] relates the transmission coefficient of the filter to the odd- and even- mode input admittances through the following formula:

$$S_{21} = Y_0 \frac{Y_{ino} - Y_{ine}}{(Y_0 + Y_{ino})(Y_0 + Y_{ine})}, \quad (17)$$

$$S_{11} = \frac{Y_0^2 - Y_{ino}Y_{ine}}{(Y_0 + Y_{ino})(Y_0 + Y_{ine})}, \quad (18)$$

where $Y_0 = 1/Z_0$ is the input and output microstrip line characteristic admittance.

By letting $S_{21} = 0$, the transmission zeros are positioned at the frequencies where

$$Y_{ine} = Y_{ino}. \quad (19)$$

Based on the above theoretical analysis, the theoretical transmission responses of the LPF with different C_3 varying from 0 pF to 0.3 pF are as shown in Fig. 7. In each of these cases, $L_1 = 18$ nh, $C_1 = 0.1$ pF, $L_2 = 2.5$ nh, $C_2 = 6$ pF, and $C_4 = 1.5$ pF. As illustrated in Fig. 7, only two transmission zeros appear on the S_{21} curve when $C_3 = 0$. In fact, (19) will be inevitably satisfied when $f = f_{z1}$ or f_{z2}, which coincides well with (13) and (14). When C_3 increases from 0, though the two transmission zeros on the left and right sides are both drawn to the lower area, the zero separation, that is, the stopband bandwidth, remains almost unchanged. Moreover, since the left transmission zero shifts to the passband with an increase in C_3, a sharpened filter transition is easily obtained. Furthermore, owing to the introduction of C_3, an extra transmission zero appears between the original two transmission zeros. This additional transmission zero also moves to the upper area with an increase in C_3. Therefore, the stopband rejection can be effectively improved by choosing a proper C_3 to properly relocate the zeros. Additionally, the change in C_3 hardly alters the filter's passband, which largely facilitates the filter design and adjustment.

III. Compact Low-Pass Filter Design

Figure 8 shows the geometry of the LPF using one of the proposed structures. The filter was fabricated on a 0.5 mm substrate with a relative dielectric constant of 2.65. The optimized dimensions of the LPF are arranged as follows: $l_u = 24.6$ mm, $w_u = 0.2$ mm, $w_{50} = 1.35$ mm, $w_m = 0.2$ mm, $w_{l1} = 0.2$ mm, $l_{l1} = 1.2$ mm, $w_{l2} = 8.1$ mm, $l_{l2} = 7.9$ mm, $s_l = 0.4$ mm, $l_{m1} = 2.7$ mm, $l_{m2} = 10.8$ mm, and $s_m = 0.3$ mm. The simulated and measured results, which show a good agreement, are illustrated in Fig. 9. This LPF has a measured 3 dB cutoff frequency of f_c at about 0.85 GHz. The measured passband insertion loss is within 0.5 dB including the SMA connector loss in the frequency range up to 0.7 GHz. The three transmission zeros can be observed to be located at 1.65 GHz with 54.5 dB, at 2.65 GHz with 67 dB, and at 3.17 GHz with 36.25 dB, respectively. The transmission zero located at

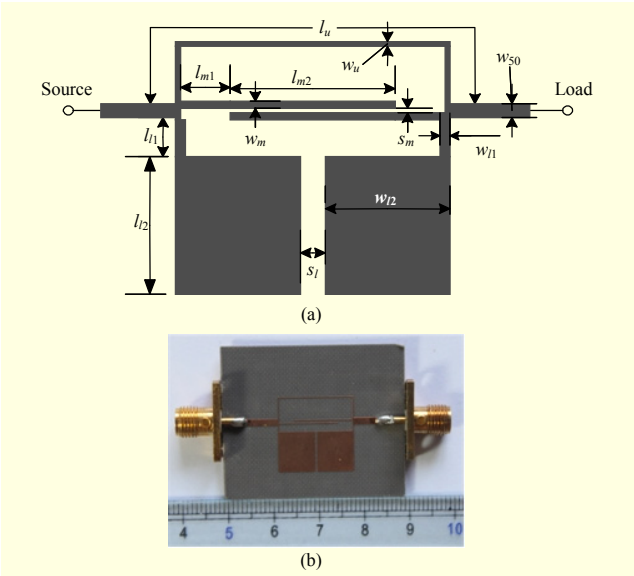

Fig. 8. Geometry of single-unit LPF: (a) layout and (b) photograph.

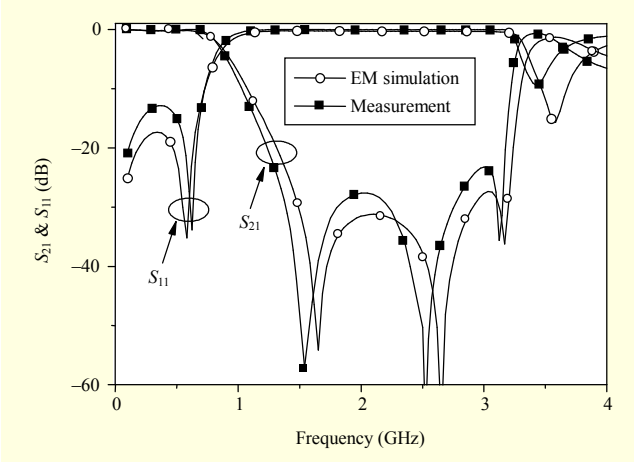

Fig. 9. Simulated and measured results of initial single-unit filter.

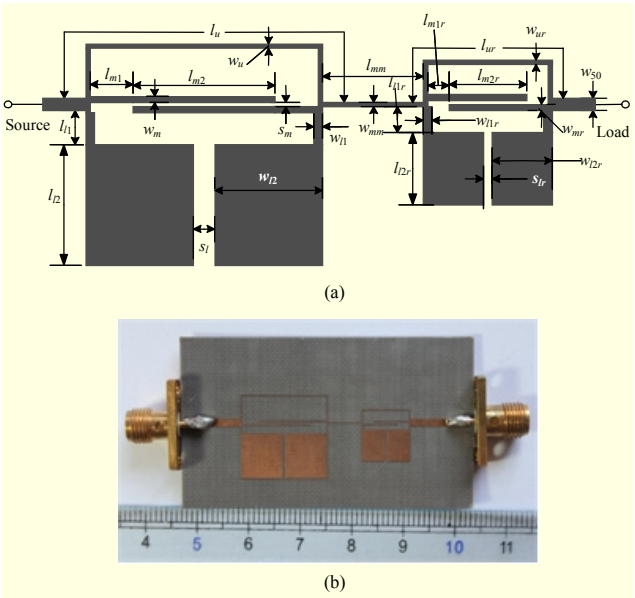

Fig. 10. Geometry of two-unit LPF: (a) layout and (b) photograph.

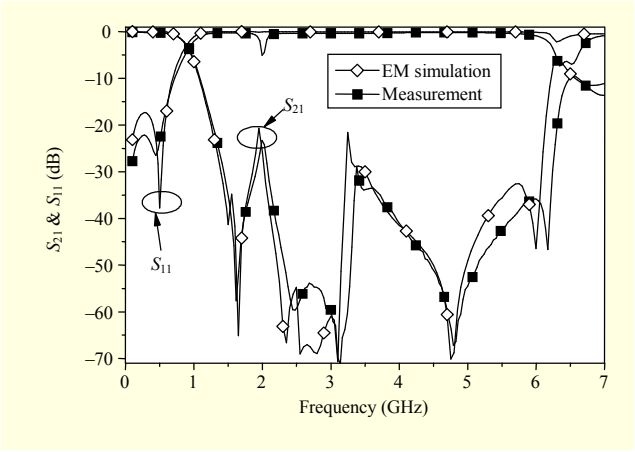

Fig. 11. Simulated and measured results of two-unit filter.

1.65 GHz contributes to a sharper transition; the one at 3.17 GHz extends the stopband; and the one at 2.65 GHz provides additional rejection between the lower and upper transmission zeros. Owing to the co-operation of these three transmission zeros, the rejection band is extended from 1.31 GHz (1.54 f_c) to 3.23 GHz (3.8 f_c) over 20 dB, resulting in a 20 dB stopband bandwidth of 2.26 f_c. Moreover, the filter occupies a compact size of 16.6 mm × 14.65 mm corresponding to $0.0042\lambda_g^2$ ($0.068\lambda_g \times 0.061\lambda_g$), where λ_g is the guided wavelength of a 50 Ω transmission line at f_c.

To obtain an even broader stopband and strengthen the stopband attention, a LPF with two cascaded asymmetrical proposed units is designed, fabricated, and tested. Figure 10 shows the LPF developed from the filter shown in Fig. 9 by cascading the second unit with different dimensions, corresponding to different cutoff frequencies and positions of the transmission zeros. The two cells are connected by a short high-impedance line with a narrow width of 0.16 mm and a length of 6.5 mm. The dimensions of the second smaller unit are l_{ur} = 12.8 mm, w_{ur} = 0.2 mm, w_{mr} = 0.2 mm, w_{l1r} = 0.2 mm, l_{l1r} = 1.1 mm, w_{l2r} = 4.5 mm, l_{l2r} = 5.6 mm, s_{lr} = 0.3 mm, l_{m1r} = 2.1 mm, l_{m2r} = 4.7 mm, and s_{mr} = 0.32 mm. This smaller-sized unit is designed to extend the stopband and suppress the harmonic resonance at around 4 GHz, as shown in Fig. 9. The smaller optimized unit has three transmission zeros at 2.68 GHz, 4.72 GHz and 5.75 GHz. The HFSS simulation and measurement are shown in Fig. 11. As shown in Fig. 11, this LPF exhibits a good low-pass response with a measured f_c at about 0.875 GHz. The filter exhibits a good passband performance with a return loss of larger than 22 dB. In addition,

Table 1. Performance comparison with some reported compact LPFs.

Reference	f_c (GHz)	20 dB stopband			Size (λ_g^2)	Minimum return loss (dB)
		f_{20dBL} (f_c)	f_{20dBU} (f_c)	BW= f_{20dBU}–f_{20dBL} (f_c)		
3	2.75	1.07	3	1.93	0.063	17
4	2.5	1.07	3	1.96	0.056	18
6	2.14	1.236	4.37	3.07	0.022	24
7	1.5	1.4	5	3.6	large	13.6
8	1.0	1.38	6	4.62	0.012	20
9	2.5	1.28	4.72	3.44	0.022	14
10	1.99	1.36	4.20	2.84	0.008	29
11	0.53	1.6	5.1	3.6	0.022	16.3
This work	0.875	1.457	7.2	5.743	0.0089	22

multiple transmission zeros can be clearly observed to be positioned at 1.62, 2.48, 3.14, 4.79, and 6.18 GHz. As a result of the effects of these multiple transmission zeros, the 20 dB rejection stopband is extended from 1.275 GHz (1.457 f_c) to 6.3 GHz (7.2 f_c) over 20 dB, indicating a very wide 20 dB stopband bandwidth of 5.743 f_c. The attenuation rates at the passband to stopband transition knees are 87 dB/GHz (the measured attenuations being 5 and 65 dB at 0.96 GHz and 1.65 GHz, respectively). Furthermore, the filter's size is only 32.4 mm × 14.65 mm, corresponding to $0.0089\lambda_g^2$ ($0.14\lambda_g \times 0.0635\lambda_g$), where λ_g is the guided wavelength of a 50 Ω transmission line at 0.875 GHz.

Table 1 shows a performance comparison of the proposed LPF with some recently reported compact and high-performance LPFs. As shown in the table, the proposed LPF in this paper exhibits a good return loss, compact size, and significantly wider stopband than the other LPFs.

IV. Conclusion

This paper presented a compact structure with three inherent transmission zeros and its application in a compact and high-performance LPF design. A theoretical analysis reveals that the stopband performance of the LPFs based on the proposed structure can be effectively upgraded by adjusting the circuit's electrical parameters to generate and reallocate the multiple transmission zeros. Finally, after a single-unit LPF was extensively studied, an improved LPF with two cascaded asymmetric units was developed. The measured results of the cascaded LPF demonstrate many desirable features as compared with a conventional LPF, particularly its ultra-wide 20 dB rejection stopband and compact size.

References

[1] G. Matthaei, L. Young, and E.M.T. Jones, *Microwave Filters, Impedance-Matching Networks, and Coupling Structures*, Boston, MA: Artech House, 1980.

[2] N.C. Karmakar and M.N. Mollah, "Investigations into Non-Uniform Photonic-Bandgap Microstripline Low-Pass Filters," *IEEE Trans. Microw. Theory Tech.*, vol. 51, no. 2, Feb. 2003, pp. 564-572.

[3] J. Yang and W. Wu, "Compact Elliptic-Function Low-Pass Filter Using Defected Ground Structure," *IEEE Microw. Wireless Compon. Lett.*, vol. 18, no. 9, Sept. 2008, pp. 578-580.

[4] D. Xi et al., "A Compact Low-Pass Filter with Sharp Cutoff and Low Insertion Loss Characteristics Using Novel Defected Grounded Structure," *Progress in Electromag. Research. Lett.*, vol. 17, Jan. 2010, pp. 133-143.

[5] L.-H. Hsieh and K. Chang, "Compact Elliptic-Function Low-Pass Filters Using Microstrip Stepped-Impedance Hairpin Resonators," *IEEE Trans. Microw. Theory Tech.*, vol. 51, no. 1, Jan. 2003, pp. 193-199.

[6] L. Li and Z.F. Li, "Compact Quasi-Elliptic Lowpass Filter Using Symmetric Rectangular Coupled Capacitors," *IET Electron. Lett.*, vol. 44, no. 2, Jan. 2008, pp. 124-125.

[7] W.-H. Tu and K. Chang, "Compact Microstrip Low-Pass Filter with Sharp Rejection," *IEEE Microw. Wireless Compon. Lett.*, vol. 15, no. 6, June 2005, pp. 404-406.

[8] L. Li, Z.-F. Li, and J.-F. Mao, "Compact Lowpass Filters With Sharp and Expanded Stopband Using Stepped Impedance Hairpin Units," *IEEE Microw. Wireless Compon. Lett.*, vol. 20, no. 6, June 2010, pp. 310-312.

[9] S. Luo, L. Zhu, and S. Sun, "Stopband-Expanded Low-Pass Flters Using Microstrip Coupled-Line Hairpin Units," *IEEE Microw. Wireless Compon. Lett.*, vol. 18, no. 8, Aug. 2008, pp. 506-508.

[10] R. Li, D.I. Kim, and C.M. Choi, "Compact Structure with Three Attenuation Poles for Improving Stopband Characteristics," *IEEE Microw. Wireless Compon. Lett.*, vol. 16, no. 12, Dec. 2006, pp. 663-665.

[11] V.K. Velidi and S. Sanyal, "Sharp Roll-Off Lowpass Filter with Wide Stopband Using Stub-Loaded Coupled-Line Hairpin Unit," *IEEE Microw. Wireless Compon. Lett.*, vol. 21, no. 6, June 2011, pp. 301-303.

Lin Li received his BS in electrical engineering from Zhejiang University, Hangzhou, China in 1999, his MS in electronic science and technology from Zhejiang University, Hangzhou, China in 2005, and his PhD in electromagnetic field and microwave technology from Shanghai Jiaotong University, Shanghai, China in 2009. His current research interests include microwave integrated circuits and antenna technologies.

Jia Bao received her BS in applicative electron technology from Anhui Normal University, Wuhu, China in 2000, and her MS in power electronics and power transmission from South West Jiaotong University, Chengdu, China in 2003. She is currently a PhD candidate of mechanical engineering at Zhejiang Sci-Tech University, Hangzhou, China. Her current research interests include embedded systems, network applications, and protocol development.

Jing-jing Du received her BS in electronic and information engineering from Harbin Engineering University, Harbin, China in 1999, and her MS in circuits and systems from Hangzhou Dianzi University, Hangzhou, China in 2006. She is currently a PhD candidate of mechanical engineering at Zhejiang Sci-Tech University, Hangzhou, China. Her current research interests include EDA, image processing, and information fusion.

Yaming Wang earned his PhD degree in biomedical engineering from Zhejiang University, China. He is currently a professor of computer science at Zhejiang Sci-Tech University, Zhejiang, China. He was a visiting researcher and visiting scientist at Hong Kong University of Science & Technology, HKUST. His current title is Dean of the School of Information Science and Technology at Zhejiang Sci-Tech University. His research interests include computer vision, pattern recognition, signal processing, and medical image processing.